Chiral Morphologies and Interfacial Electronic Structure of Naphtho[2,3-a]pyrene on Au(111)

C. B. France[†] and B. A. Parkinson*[,‡]

Colorado State University, Department of Chemistry, Fort Collins, Colorado 80523, and Intel Corporation, Portland Technology Development, Hillsboro, Oregon 97124

The adsorption of the two-dimensionally chiral naphtho[2,3-a]pyrene molecule has been studied on Au(111). Both structural and electronic properties of the naphtho[2,3-a]pyrene (NP)/Au(111) interface have been measured. Ultraviolet and X-ray photoelectron spectroscopy have been employed to measure the energies of the molecular orbitals of the NP film with respect to the gold Fermi level. A Schottky junction with a large interface dipole (0.99 eV) is formed between Au(111) and NP. Temperature-programmed desorption was used to determine that adsorbed NP has a binding energy of 102.2 kJ/mol. Chiral domains have been observed with scanning tunneling microscopy due to the spontaneous phase separation of the 2-D enantiomers. Two distinct structural polymorphs have been observed, one of which has homochiral paired molecular rows. Models of the 2D structure are proposed that are in excellent agreement with experimental measurements.

Introduction

Stereospecific chemistry is important for the synthesis, detection, and separation of enantiopure compounds. Essential biomolecules, biological structures, and some naturally occurring minerals contain chiral configurations that are of scientific and industrial importance. A surface that can sense, separate, or selectively catalyze these chiral centers would be of great utility. The production of chiral surfaces is limited by the ability to generate the handedness of the desired substrate materials. There are at least three different approaches that can be used to form a chiral surface. The first is the use of naturally occurring chiral surfaces, such as certain high-index metal surfaces.[1] This approach has the advantage that the crystalline surface is inherently chiral; however, it will be difficult to tailor the surface to bind a specific adsorbate. These kinds of surfaces can selectively adsorb one enantiomer,[1] but further geometric specificity for molecular recognition and sensor applications will be difficult to achieve.

The second and third techniques for generating a chiral surface involve the use of an achiral surface and the deposition of adsorbates that form chiral structures on the surface. The adsorption of chiral molecules can produce chiral patches of exposed substrate in the spaces between the adsorbates. In these spaces, the substrate surface remains exposed; only chiral molecules of a desired enantiomer with the correct geometric specificity can be bound at the asymmetric patches. The chiral surface pockets can then be tailored by changing the initial adsorbate or its surface coverage, allowing for increased selectivity of the molecules being "sensed". While more primitive than nature's enzyme/substrate lock and key mechanism, this method has the potential to allow for the development of similar catalytic stereospecificity. The formation of a chiral surface has been produced through the deposition of 3D chiral molecules on low-index metal surfaces.[2,3] These procedures have the drawback that

enantiomeric pure forms of the initial adsorbate must be available. We are currently investigating the third method of producing a chiral surface based on the use of achiral adsorbates that have two-dimensional chirality. While these molecules are not chiral in three dimensions, adsorption to a surface results in the loss of mirror plane symmetry, leading to nonsuperimposable forms of the molecules on the surface. Local chiral pockets can be formed if the 2D enantiomers phase segregate; however, the entire surface will not be stereoselective unless one enantiomeric domain is somehow favored over the other.

Scanning tunneling microscopy (STM) has been used to characterize chiral structures on surfaces produced by organic adsorbates. Racemic mixtures of chiral adsorbates have been found to segregate into pure *R* or *S* enantiomeric domains at the liquid/solid interface.[4] DL-Cysteine has been observed to form racemic domains of homochiral pairs on Au in a vacuum environment. Additionally, two-dimensionally chiral molecules have also been observed to produce chiral domains. Systems using covalently bound adsorbates,[5] metal−organic complexes,[6] organic acids with long alkane tails,[7] hydrogen bonding functional groups,[8] and helical heptahelicene molecules[9] have been recently reported.

In this contribution, we have utilized X-ray and ultraviolet photoelectron spectroscopy (XPS and UPS) to measure an approximate energy level diagram of naphtho-[2,3-a]pyrene (NP) (the molecular structure of NP is presented in the upper right of Figure 1) on Au(111). The binding energy of NP to Au(111) was measured utilizing temperature-programmed desorption (TPD), and STM was

---

* To whom correspondence should be addressed. E-mail: bruce.parkinson@colostate.edu. Fax: (970) 491-1801.
[†] Intel Corp.
[‡] Colorado State University.

(1) Horvath, J. D.; Gellman, A. J. *J. Am. Chem. Soc.* **2001**, *123*, 7953.
(2) Chen, Q.; Lee, C. W.; Frankel, D. J.; Richardson, N. V. *PhysChemComm* **1999**, *9*, 05986.

(3) Nakanishi, T.; Yamakawa, N.; Asahi, T.; Osaka, T.; Ohtani, B.; Unosaki, K. *J. Am. Chem. Soc.* **2002**, *124*, 740.
(4) Fang, H.; Giancarlo, L. C.; Flynn, G. W. *J. Phys. Chem. B* **1998**, *102*, 7311.
(5) Ohtani, B.; Shintani, T.; Uosaki, K. *J. Am. Chem. Soc.* **1999**, *121*, 6515.
(6) Messina, P.; Dmitriev, A.; Lin, N.; Spillmann, H.; Abel, M.; Barth, J. V.; Kern, K. *J. Am. Chem. Soc.* **2002**, *124*, 14000.
(7) Yablon, D. G.; Giancarlo, L. C.; Flynn, G. W. *J. Phys. Chem. B* **2000**, *104*, 7627.
(8) Barth, J. V.; Weckesser, J.; Trimarchi, G.; Vladimirova, M.; De Vita, A.; Cai, C.; Brune, H.; Gunter, P.; Kern, K. *J. Am. Chem. Soc.* **2002**, *124*, 7991.
(9) Fasel, R.; Parschau, M.; Ernst, K.-H. *Angew. Chem.* **2003**, *115*, 5336.
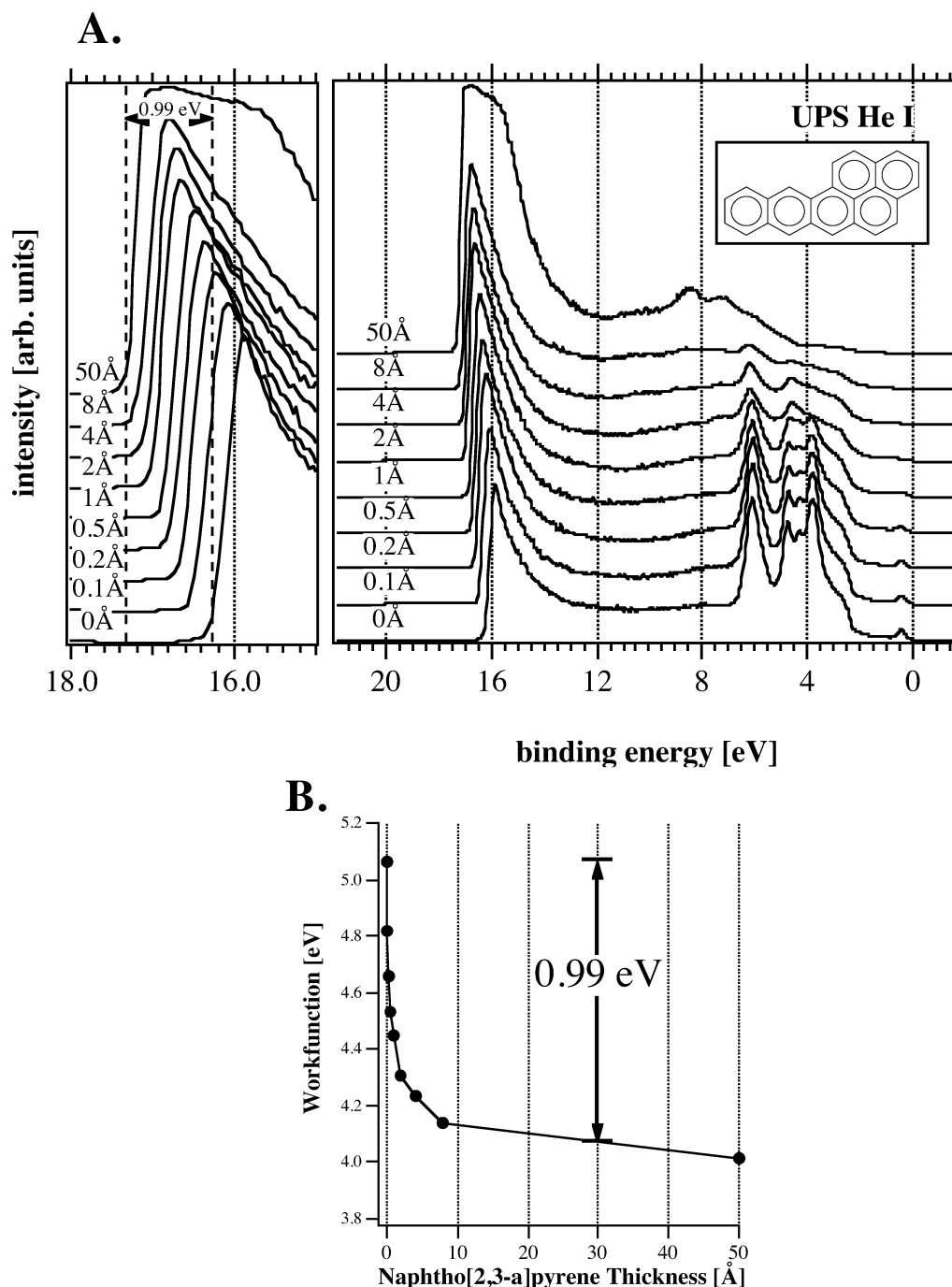

A.

binding energy [eV]

B.

Figure 1. (A) UPS He I spectra of naphtho[2,3-a]pyrene deposited on Au(111). The right portion shows the full spectra on a binding energy scale. The high binding energy cutoff is shown on the left. The molecular structure of NP is shown in the upper right of the figure. (B) A plot of the interface work function versus the NP film thickness. The total work function shift was determined to be 0.99 eV.

used to observe the 2D structures formed by NP. Proposed structural models of the ordered domains are presented. While numerous morphological and electronic studies have been undertaken on adsorbed symmetric aromatic molecules,[10−18] to our knowledge this is the first observation of a two-dimensional chiral aromatic system.

Experimental Section

Experiments were performed in a commercial Omicron Multi-probe ultrahigh vacuum (UHV) system (base pressure, 5×10^{-11} mbar). This system is equipped with a variable temperature scanning tunneling microscope (VT-STM) for structural characterization.[19] XPS and UPS using a VSW EA125 single-channel hemispherical analyzer were used to study the electronic structure of the interface. TPD has been added to the UHV system

(10) France, C. B.; Parkinson, B. A. *Appl. Phys. Lett.* **2003**, *82*, 1194−1196.

(11) France, C. B.; Schroeder, P. G.; Forsythe, J. C.; Parkinson, B. A. *Langmuir* **2003**, *19*, 1274.

(12) France, C. B.; Schroeder, P. G.; Parkinson, B. A. *Nano Lett.* **2002**, *2*, 693.

(13) Schroeder, P. G.; France, C. B.; Park, J. B.; Parkinson, B. A. *J. Appl. Phys.* **2002**, *91*, 3010.

(14) Schroeder, P. G.; France, C. B.; Park, J. B.; Parkinson, B. A. *J. Phys. Chem. B* **2003**, *107*, 2253.

(15) Schroeder, P. G.; France, C. B.; Parkinson, B. A.; Schlaf, R. *J. Appl. Phys.* **2002**, *91*, 9095.

(16) Schroeder, P. G.; Nelson, M. W.; Parkinson, B. A.; Schlaf, R. *Surf. Sci.* **2000**, *459*, 349.

(17) Lackinger, M.; Griessl, S.; Heckl, W.; Hietschold, M. *J. Phys. Chem. B* **2002**, *106*, 4482.

(18) Schlaf, R.; Parkinson, B. A.; Lee, P. A.; Nebesny, W.; Armstrong, N. R. *J. Phys. Chem. B* **1998**, *103*, 2984.

as previously described.[11] A physical vapor deposition chamber (base pressure, 1×10^{-9} mbar) is attached to the UHV system allowing samples and films to be prepared in situ.

The gold film was prepared by heating a 1 cm × 1 cm mica sample, attached to the sample plate using molybdenum clips, for 24 h in UHV at 300 °C to evaporate surface contaminants. Gold was then evaporated from a resistively heated tungsten basket onto the heated mica substrate.[20] The Mo clips provide electrical contact to the gold surface during STM imaging. Sputter (2 keV Ar$^+$) and anneal (350 °C) cycles were used to clean and flatten the Au(111) surface. The chemical purity of the surface was determined with XPS (Mg Kα, 50 eV pass energy), and the presence of the $23 \times \sqrt{3}$ reconstruction was confirmed with STM.[21]

NP (Aldrich Chemical Co.) films were deposited under UHV (base pressure, 1×10^{-9} mbar) from a resistively heated boron nitride crucible (source temperature, ~100 °C). The source was maintained at 75 °C for 12 h prior to deposition to remove any volatile contaminants. The crucible containing naphtho[2,3-a]-pyrene was heated to obtain a desired deposition rate that was monitored by a Leybold quartz crystal microbalance (QCM). The Au(111) substrate was maintained at room temperature during the deposition.

Sequential depositions were performed up to a final film thickness of 50 Å. After each growth step, XPS (Mg Kα, 50 eV pass energy) and UPS (HeI, 21.21 eV; and HeII, 40.81 eV; both with 10 eV pass energy) in normal emission were utilized to measure the electronic structure of the surface. A −5.00 V bias was applied to the sample for the UPS measurements to separate the sample and spectrometer high binding energy cutoffs (HBECs). The spectrometer was calibrated as previously described.[14] Work function and highest occupied molecular orbital (HOMO) cutoff positions were determined from the high binding energy cutoffs and HOMO onsets of UP spectra and were corrected for the analyzer broadening by adding/subtracting 0.1 eV. XPS core level peak positions were determined by using an IGOR Pro (Wavemetrics) data evaluation software fitting routine. A vacuum-deposited naphtho[2,3-a]pyrene film on quartz was used to obtain the solid-state absorption spectrum that was measured using a Varian Cary-500 UV−vis−NIR spectrophotometer.

The STM was performed in constant current imaging mode with typical sample biases of −0.5 V and tunneling currents between 0.1 and 0.5 nA. The Au(111) surface was renewed before each STM experiment with a sputter and anneal cycle. NP films of various thicknesses were then deposited on the cleaned surface. A background plane fit or slope correction was the only postcollection processing applied to the images with the exception of Figure 10B, which was processed with a correlation-averaging algorithm utilizing Scanning Probe Image Processing (SPIP) software (Image Metrology Aps.).

Results and Discussion

The orbital energy alignment between Au(111) and NP was measured utilizing photoemission spectroscopies. A clean Au(111) sample was prepared by sputtering and annealing and characterized with both UPS and XPS. NP was then deposited and analyzed in eight steps to a final thickness of 50 Å. The He I UPS spectra of NP on Au(111) are presented in Figure 1A, where the full spectra are on the right of the figure and the normalized zoom-in of the HBEC is shown on the left. The bottom-most spectrum is of the clean Au(111) sample, and each subsequent deposition step is shown above it. Changes in the band structure are evident as the NP film thickness increases. The existence of a large interface dipole is suggested by the significant shift in the HBEC between the bare gold sample and the 8 Å NP film. The work function of the gold substrate was determined by subtracting the HBEC of
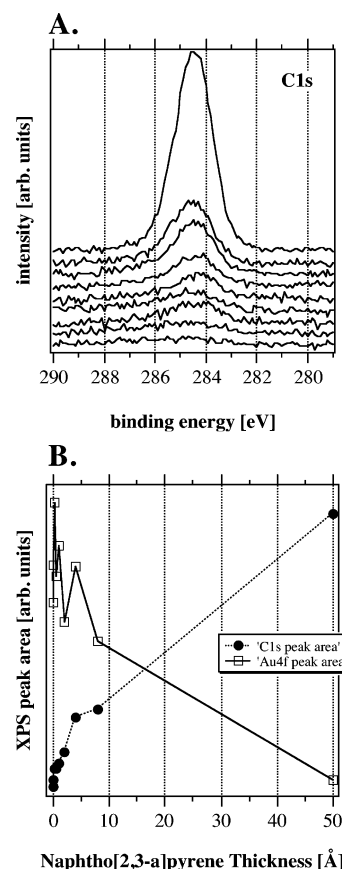

Figure 2. (A) C1s XPS of naphtho[2,3-a]pyrene with increasing film coverage. (B) Plot of the C1s (filled circles) and Au4f (open squares) peak area versus NP film thickness.

the UP spectra from the source energy (21.22 eV) yielding Φ = 5.06 eV. This work function is slightly lower than published values for single-crystal Au(111);[22] however, this sample is a Au film on mica that contains other Au orientations. The work function of the film after deposition of 8 Å of NP is determined to be 4.07 eV. The total work function shift of 0.99 eV between the clean gold work function and the 8 Å film of NP represents a good approximation of the interface dipole formed by the NP on Au(111). The shift in the work function as a function of NP film thickness is plotted in Figure 1B.

To monitor the chemical purity and determine if the film is charging during these experiments, atomic core level spectra were measured with XPS.[15,16,23] A complete band lineup was determined; however, band bending or polarization related shifts are not included as these experiments did not proceed to thick enough films. High-resolution C1s XP spectra for NP on Au(111) are shown in Figure 2A. No peak shift within the limit of the analyzer resolution (0.2 eV) is observed, and the peak energy at all coverages was 284.4 ± 0.1 eV. Peak areas linearly increased with NP film coverage. A plot of the C1s and Au4f peak areas versus NP film thickness, as determined by QCM, is shown in Figure 2B. The 50 Å NP film is not of uniform thickness since the Au XPS peaks can still be detected through the 50 Å NP film. The electron escape depth of the Au core level electrons should be less than 20 Å,[24] indicating islanding or uneven growth of the organic film.

(19) The variable temperature capabilities of this instrument were not utilized during these experiments. All STM images in this report were produced at room temperature.
(20) The gold film thickness on the mica is estimated at a few microns.
(21) Barth, J. V.; Brune, H.; Ertl, G.; Behm, R. J. *Phys. Rev. B* **1990**, *42*, 9307.

(22) *Handbook of Chemistry and Physics*, 74th ed.; Lide, D. R., Ed.; CRC Press: Boca Raton, FL, 1994.
(23) Schlaf, R.; Schroeder, P. G.; Nelson, M. W.; Parkinson, B. A.; Lee, P. A.; Armstrong, N. R. *J. Appl. Phys.* **1999**, *86*, 1499.
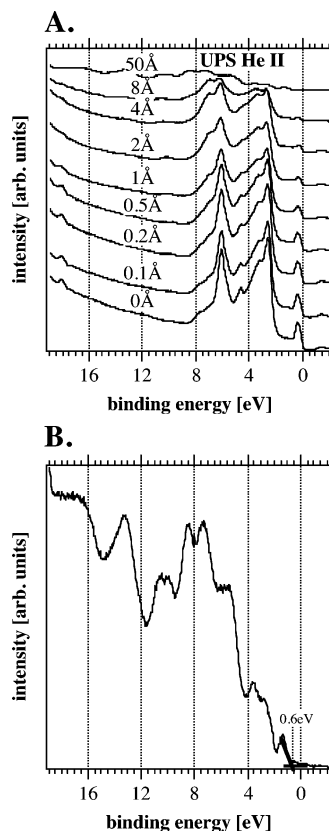
A.

B.

Figure 3. (A) UPS He II spectra of naphtho[2,3-a]pyrene on Au(111). (B) Expanded He II spectrum of 50 Å thick NP film.

UPS He II spectra were obtained to determine the valence states of the interface. Figure 3A shows the He II spectra that were measured during the growth of the NP film. The bottom spectrum is the clean Au(111) film on mica. Subsequent depositions of the aromatic molecule show the valence states of the gold are gradually replaced by the spectrum of the organic film. No gas-phase photoelectron data for NP are currently available to aid in interpretation of this spectrum. The gold states in the spectra are completely obscured with a 50 Å coverage of NP. This thick film He II UP spectrum is shown in Figure 3B. For the thick film, no states are observed at the Fermi energy (0 eV); however, the HOMO of the NP film is observed as the lowest binding energy edge of the spectrum and has an onset at 0.6 eV. The offset between the gold Fermi level and the HOMO cutoff of the NP is of interest because it represents the height of the hole injection barrier (E_{bh}) at the interface ($E_{bh} = 0.6$ eV).

The position of the lowest unoccupied molecular orbital (LUMO) cannot be measured directly with XPS or UPS; however, it can be estimated by determining the lowest energy optical absorption of a thin solid-state film of NP. The visible absorption spectrum of a solid-state NP film that was evaporated onto a quartz slide is shown in Figure 4. The lowest energy absorption maximum occurs at 510 nm, corresponding to a band gap (E_{bg}) of 2.42 eV. (It is important to note that the optical band gap is only used as an estimate for the HOMO−LUMO gap since the large excitonic binding energy is not accounted for and the absorption maximum rather than onset is used.)[25] The estimated band gap for NP allows for the determination
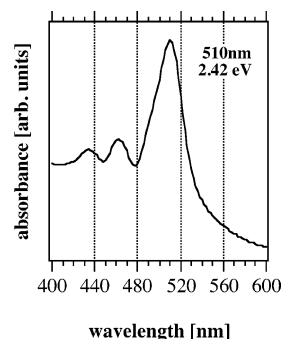
(24) Wagner, C. D.; Riggs, W. M.; Davis, L. E.; Moulder, J. F.; Muilenberg, G. E. *Handbook of X-ray photoelectron spectroscopy*; Perkin-Elmer Corp.: Eden Prairie, MN, 1979.

(25) Pope, M.; Swenberg, C. E. *Electronic Processes in Organic Crystals and Polymers*; Oxford University Press: Oxford, 1999.

Figure 4. Optical absorption spectrum of a naphtho[2,3-a]-pyrene film used to estimate the band gap.
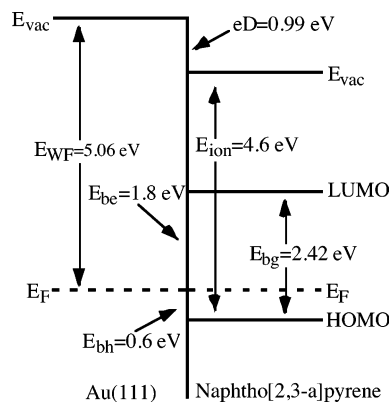

Figure 5. Band diagram of the naphtho[2,3-a]pyrene/Au(111) interface.

of the energy level position of the NP LUMO states with respect to the gold Fermi level by subtracting E_{bg} (2.42 eV) from E_{bh} (0.6 eV). This analysis also yields the magnitude of the barrier for electron injection into the organic material at the interface ($E_{be} = 1.8$ eV). The ionization potential of naphtho[2,3-a]pyrene was determined by adding the work function of the 50 Å NP film (4.0 eV) to the HOMO cutoff (0.6 eV) of the same spectra, yielding 4.6 eV. All of these energy values provide an estimate of the band lineup for naphtho[2,3-a]pyrene on Au(111) since these measurements do not include the determination of polarization or band bending related shifts. This information is graphically summarized in the energy diagram of Figure 5. The NP/Au(111) interface has a slightly larger interface dipole (0.04 eV larger) than that found at the pentacene/Au(111) interface.[14] The optical HOMO−LUMO gap of NP is also larger than that of pentacene leading to a much larger electron injection barrier (0.5 eV greater). The hole injection barrier of both interfaces is similar.

The binding energy of the naphtho[2,3-a]pyrene to the gold surface was probed with TPD. The molecular mass of NP was too large (302 amu) to detect with our mass spectrometer; therefore, a lower mass-to-charge ratio was used for these experiments. The mass monitored during TPD of the NP film desorption was at one-half its principal mass-to-charge ratio. This peak most likely represents a doubly charged intact molecule since a symmetric fragment of this intensity is unlikely for this asymmetric molecule. The strong doubly charged parent peak and the identical optical absorbance of evaporated films and nonvacuum prepared films demonstrate that the molecule remains intact during deposition. Additionally, the NP molecules are observed to remain intact on the Au(111) in the STM experiments discussed below.

Unlike previous experiments with organic semiconductor interfaces on Au(111),[10,11] we were only able to resolve
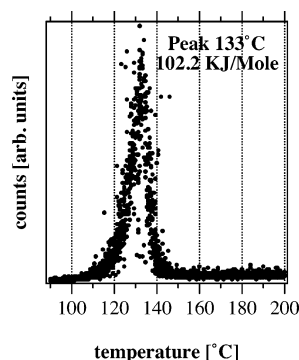
Figure 6. Representative temperature-programmed desorption peak of naphtho[2,3-a]pyrene on Au(111). The peak temperature of NP is 133 °C, which corresponds to a binding energy of 102.2 kJ/mol.

one TPD peak with the NP/Au(111) system. TPD experiments were conducted at a number of different initial NP film coverages; however, all spectra were similar to the one presented in Figure 6. This spectrum was obtained from a 50 Å thick film; however, with the exception of the signal-to-noise, it is comparable to those obtained at lower initial film coverages. The base of the TPD peak appears fairly wide (>20°C range) and has a comparable width to the monolayer peak of pentacene on Au(111) that has contributions from a number of different structural polymorphs.[11] Several possibilities could explain the single binding energy peak. First, the fact that multiple peaks were not resolved simply indicates that the multilayer and monolayer binding energies are almost identical. Second, the similar energies could be the result of the multilayer/bulk crystal structure that is formed by NP. Pentacene and *p*-sexiphenyl that have different crystal and surface energies have similar crystal packings.[10,11] Thus if NP forms a stronger crystalline packing it may have a sublimation energy nearly identical to the binding energy of NP molecules in contact with the Au(111). Finally, the desorption mechanisms of the asymmetric and symmetric organic adsorbates may differ. The temperature of the NP desorption peak was determined to be 133 °C, corresponding to a binding energy of 102.2 kJ/mol.[26] This value is similar to that obtained for pentacene (106 kJ/mol bulk and 110 kJ/mol multilayer), which has a similar molecular structure.[11] However, the higher vapor pressure of NP compared with pentacene (∼100 °C deposition versus 142 °C for pentacene) suggests a stronger interaction with the Au(111).

Scanning tunneling microscopy was utilized to image the surface structures of NP on Au(111). As was found with other aromatic adsorbates,[10–12] NP did not lift the Au(111) 23 × √3 reconstruction since the elevated herringbone reconstruction can be seen through the organic film in the STM image in Figure 7A and in many other STM images. The reconstruction traverses the small ordered NP domain in the [11$\bar{2}$] direction. Reconstruction elbows are present at the top of the figure where the ordered domain terminates. Disordered mobile NP molecules, moving faster than the time scale of the imaging process, cause the noisy region around the ordered domain.[27] A second STM higher resolution image on the boundary region between the ordered and mobile areas is shown in Figure 7B. The bright or high spots in the image represent the NP molecules. Careful inspection of these imaged molecules shows the characteristic shape of
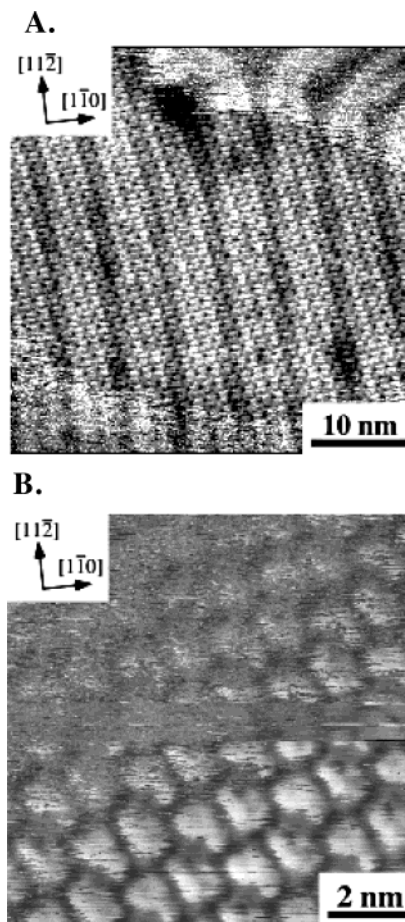
(26) Redhead, P. A. *Vacuum* **1962**, *12*, 203.
(27) Berner, S.; Brunner, M.; Ramoino, L.; Suzuki, H.; Güntherodt, H.-J.; Jung, T. A. *Chem. Phys. Lett.* **2001**, *348*, 175.


Figure 7. (A) STM image of the NP domain on Au(111). The 23 × √3 reconstruction is visible traveling vertically in the image. (B) Zoom-in of the ordered mobile boundary of the chiral NP domain.

one of the enantiomers of the two-dimensionally chiral NP molecules, the shape of a backward "P". All of the NP molecules in this image are the same 2D enantiomer as indicated by the fact the molecules are superimposable with either a translation or a simple 180° rotation within the plane of the surface. The fact that only one enantiomer is present in this domain indicates that the two forms of the NP molecule have segregated and formed chiral domains on the Au(111) substrate. The molecules at the top of the STM image in Figure 7B are noisier than those at the bottom, which is a result of molecules moving at the edges of the ordered domain. Molecules further away (at the top of the image) spend less time ordered in the structure and therefore appear noisier and fainter than those at the bottom, that have an increased residence time in the chiral domain.[27]

An additional STM image of the chiral NP domain is presented in Figure 8A with space filling models of the NP molecules shown in Figure 8B to help the reader more easily see the molecules' orientation in this chiral domain. These two high-resolution images reveal the shapes of the individual molecules. Crossing the image from left to right, the molecular orientation alternates within a row, with one having the naphtho group pointing down and the next pointing up. Perpendicular to these rows, the dark regions (where the Au(111) is exposed) have an "S" shape to them, as opposed to a "Z" shape that would be characteristic of the mirror image domain. Z-Shaped domains have also been observed in STM images of NP on Au(111) indicating the formation of enantiomeric segregated domains of two-dimensionally chiral molecules.
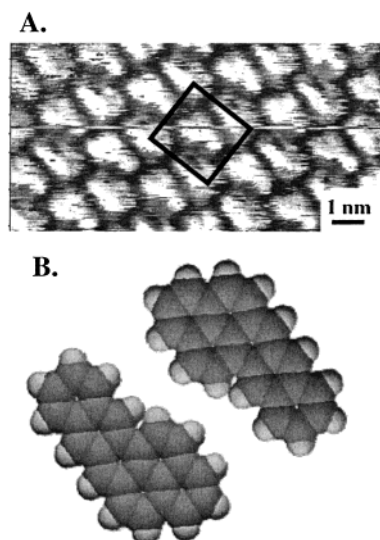
Figure 8. (A) Unit cell of chiral domain is outlined by a black box. (B) Space filling models of NP to show the orientation of molecules.
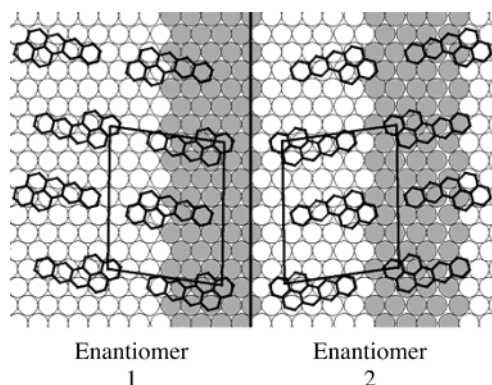

Figure 9. Proposed model of enantiomeric domains formed by 2D chiral naphtho[2,3-a]pyrene.

As described above, these chiral pockets of exposed metal surface could easily be influenced by changing the organic packing density, orientation, or molecules of the film, thus tailoring the shape for a second molecule to fit into the pocket to be sensed or undergo a catalytic reaction.

The unit cell is drawn as the black square in Figure 8B. The measured short unit cell distance, along the direction where the NP molecules have an end-to-end nearest neighbor interaction, averaged 16.3 Å with a standard deviation of ± 0.4 Å ($a = 16.3 \pm 0.4$ Å). The long unit cell distance averaged 19.4 Å with a standard deviation of ± 1.0 Å ($b = 19.4 \pm 1.0$ Å). The unit cell angle between a and b is $50 \pm 3°$. The angle between the reconstruction direction [11$\bar{2}$] and the a unit cell direction was measured to be $86 \pm 2°$.

A proposed model structure of the chiral domains is presented in Figure 9. The modeled unit cell contains two molecules, is representative of the chiral plane group $p2$, and has a theoretical packing density of 6.25×10^{13} molecules/cm². The domain is modeled with the terminal rings of the molecules located on atop sites of the gold surface; although we have not directly observed this level of detail, the orientation of the molecules with respect to the reconstruction is consistent. Our previous studies of large symmetric aromatic molecules, as well as other investigations, suggest that molecules prefer to center the largest possible number of aromatic rings directly above Au atoms.[10-13,28] The model unit cell parameters are compared with the experimental measurements in
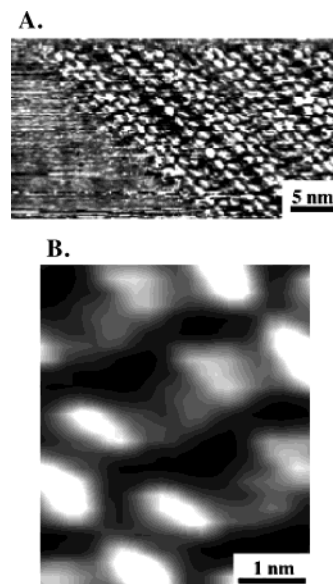

Figure 10. (A) STM image of the NP homochiral paired row domain on Au(111). (B) Zoom-in STM image of the homochiral paired row structure obtained utilizing the correlation-averaging algorithm in the SPIP software.

Table 1. Experimentally Measured and Modeled Parameters for the Chiral Domains Formed by Naphtho[2,3-a]pyrene Molecules on Au(111)

parameter	experimental	modeled
a	16.3 ± 0.4 Å	16.1 Å
b	19.4 ± 1.0 Å	19.9 Å
α	$50 \pm 3°$	50.2°
$\angle a$, reconstruction	$86 \pm 2°$	81°
$\angle$ enantiomeric domains	$163 \pm 5°$	162°

Table 1. Furthermore, the model predicts that chiral domains should intersect at an angle of 162° (between adjacent unit cell vectors) as was also observed in STM images. All modeled parameters are shown to be in good agreement with the experimentally measured distances and angles.

A second structure, containing homochiral pairs, has also been observed with STM albeit with lower resolution. We believe this structure, while not conclusively observed in STM images like above, is significant because of the formation of paired row structures reminiscent of those observed for symmetric aromatic adsorbates on Au.[11,29] It is important to note that this structure is not commonly imaged and high-resolution images like those shown in Figure 8 have not been obtained. However, enough information has been gathered about this structure from many lower resolution images that a model has been developed that is supported by the thorough analysis and high-resolution images of the previously discussed structure. An STM image of the paired structure is presented in Figure 10A where the upper right of the image is the ordered domain and the lower left is a noisy region of mobile molecules. The NP molecules appear as bright spots in the image with the molecules aligning themselves with the long axis of the molecule just left of vertical. The NP molecules order into a type of superstructure where clusters of two to four end-to-end rows lie next to each other. The fundamental building block of this structure is shown in Figure 10B. This is a zoom-in image of the structure in Figure 10A, obtained utilizing the correlation-

(28) Kasaya, M.; Tabata, H.; Kawai, T. *Surf. Sci.* **1998**, *400*, 367.
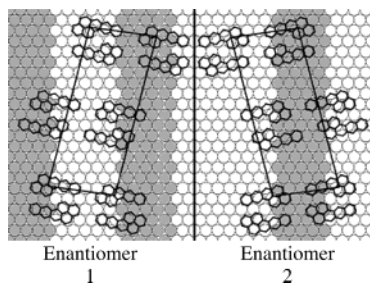(29) Frame, F. A.; France, C. B.; Parkinson, B. A. Unpublished, 2003.

Figure 11. Proposed model for the homochiral paired row domain.

Table 2. Experimentally Measured and Modeled Parameters for the Homochiral Paired Row Domain Formed by Naphtho[2,3-a]pyrene Molecules on Au(111)

measurement	experimental	modeled
a	17.0 ± 0.8 Å	16.1 Å
b	40.3 ± 2.7 Å	38.8 Å
$\angle\, a, b$	$96.2 \pm 5.2°$	96.1°
$\angle\, a$, reconstruction	$98 \pm 5°$	99°
$\angle$ enantiomeric domains	$163 \pm 5°$	161°

averaging algorithm in the SPIP software package. The pairing of the molecules into rows with the long axis of the molecule pointing in the row direction is clearly evident. Some of the molecules imaged in both panels A and B of Figure 10 have larger ends, suggesting the orientation of the molecule by way of the location of the pyrene group. Analysis of a number of images of this structure shows that the paired rows adjacent to each other are slightly offset, thus making the long axis of the unit cell encompass two paired rows. The offset is not always observed, and the energy difference between separated rows being offset or not is likely to be quite small. The measured distances of the long axis of this unit cell (over two rows) was $b = 40.3 \pm 2.7$ Å. The short axis unit cell distance, which corresponds to the length of the NP molecule, is $a = 17.0 \pm 0.8$ Å. This measurement is the same, within the standard deviation of the two measurements, as the a-axis of the previous structure. The unit cell angle was determined to be $96 \pm 5°$, and the angle between the a-axis and the Au(111) reconstruction ($[11\bar{2}]$) was $98 \pm 5°$. Different domains, thought to be composed of different enantiomers, had an a-axis angle between them of $163 \pm 5°$, again nearly identical to the enantiomeric domain boundary angle shown in the first chiral structure.

A proposed model for this homochiral paired row structure is presented in Figure 11. The dark substrate atoms represent the elevated atoms of the $23 \times \sqrt{3}$ reconstruction. The modeled unit cell parameters are presented in Table 2 and shown to be in good agreement with the experimentally measured values. The molecules interact with the underlying gold atoms in the same manner as the uniform structure (described above). The homochiral pairing of the molecules in this structure is

shown in the model. The plane group symmetry of this structure is also $p2$, and the theoretical packing density is 6.41×10^{13} molecules/cm², only 2.5% higher than that of the unpaired structure. It is unclear why the molecules form these paired rows; however, this type of interaction has been observed in symmetric aromatic molecules of p-sexiphenyl and low coverages of pentacene on Au-(111).[11,29] The parameters of the model for this paired row structure are all in agreement with the experimentally measured distances and angles.

Summary

We have characterized the electronic structure of the interface of the low-symmetry 2D chiral aromatic naphtho-[2,3-a]pyrene molecule on Au(111) using UPS and XPS. Optical absorbance of a solid-state film of NP was used to estimate the HOMO−LUMO band gap of the organic material. The band lineup of NP on Au(111) was determined, showing that a Schottky barrier is formed between these materials, with electron and hole injection barriers of 1.8 and 0.6 eV, respectively. A large interface dipole of 0.99 eV was measured at the immediate interface. TPD has been used to determine the binding energy of the NP on the metal surface. One peak was observed with a peak temperature of 133 °C corresponding to a binding energy of 102.2 kJ/mol. Two different structural polytypes both showing chiral domains have been observed with scanning tunneling microscopy. High-resolution images of the first polytype show that the domains are comprised of a single 2D enantiomeric form of NP with uniform packing of the NP molecules producing ordered domains with nearest neighbor molecules alternating by a rotation of 180°. A model has been proposed showing the ordered chiral domains as well as the interaction of the NP molecules with the hexagonal Au(111) lattice. A second, paired row structure has also been observed. The interaction with the substrate is identical to the uniform polytype; however, the molecules form homochiral-paired rows across the surface. A model has been proposed that is in agreement with experimental measurements.

These chiral domains have spontaneously formed on a hexagonal low-index metal surface. The ordered structures have formed without strong interactions between molecules such as hydrogen bonding or chemical bonds with the gold substrate. The dynamics of the chiral domain formation via surface diffusion or molecular "flipping" is currently under study. The spaces between the molecules form chiral "pockets" or "patches" that may be selective for the adsorption of specific 3D enantiomers. Such chiral recognition may be important for the future development of sensors for optically active molecules or enatioselective catalysis.

LA035532I